Alginate-honey bioinks with improved cell responses for applications as bioprinted tissue engineered constructs

Sudipto Datta, Ripon Sarkar, and Veena Vyas
Centre for Healthcare Science and Technology, Indian Institute of Engineering Science and Technology Shibpur, Howrah-711103, W.B., India

Sumant Bhutoria
Alfatek Systems, Kolkata-700033, W.B., India

Ananya Barui
Centre for Healthcare Science and Technology, Indian Institute of Engineering Science and Technology Shibpur, Howrah-711103, W.B., India

Amit Roy Chowdhury
Centre for Healthcare Science and Technology, Indian Institute of Engineering Science and Technology Shibpur, Howrah-711103, W.B., India; and Department of Aerospace Engineering and Applied Mechanics, Indian Institute of Engineering Science and Technology Shibpur, Howrah-711103, W.B., India

Pallab Datta[a)]
Centre for Healthcare Science and Technology, Indian Institute of Engineering Science and Technology Shibpur, Howrah-711103, W.B., India

(Received 28 March 2018; accepted 1 June 2018)

The polysaccharide alginate has received most extensive attention as bioink in bioprinting applications due to its ability to undergo gelation under cell-friendly conditions. However, absence of cell-binding motifs and the erratic degradation of alginate hydrogels have remained their persistent limitations. Honey is a conveniently available natural material, known for its role in wound healing and skin tissue regeneration. However, honey blending to improve biological response of alginate-based bioprinted scaffolds has not been yet reported. In the present work, honey-alginate bioinks were evaluated for their printability property (shape fidelity). It was found that honey blending reduced alginate viscosity, which gradually affected bioprinting fidelity. Therefore, the concentration that provides for acceptable bioprinting along with improvement in cell proliferations is determined. It is concluded that honey blending improves cell response of alginate bioinks and can be a facile approach to obtain bioinks especially for in situ skin tissue engineering applications.

I. INTRODUCTION

In the last few years, 3D printing has emerged as a promising fabrication method to generate engineered tissue constructs for both in vitro disease modeling and tissue engineering applications.[1] Bioprinting has further expanded the domain in which live cells can be deposited according to desired structure, shape, and cell-biomaterial compositions.[2] These techniques leverage a computer-controlled device to dispense biomaterials and/or cells into accurate, anatomically complex structures.[3,4] Although several technology platforms are now available for fabricating tissue constructs by bioprinting, extrusion-based bioprinting has emerged as a conveniently scalable, versatile, and affordable technique to generate mechanically robust tissue-engineered constructs.[4–6] Developments in bioprinting instrumentation have also led to in situ skin and cartilage tissue engineering applications.[7–9] In bioprinting, the biomaterials mostly hydrogels and the living cells together form the bioink, which is solidified to produce the constructs. The success of bioprinting is intricately related to the availability of suitable bioinks which allow bioprintability with favorable cellular responses. However, the present repertoire of bioinks provides much scope for improving their physicochemical as well as biological properties to meet the clinical challenges.[10–12]

Amongst various hydrogels, alginate, a naturally occurring polysaccharide composed of repeating units of β-D-mannuronic acid and α-L-guluronic acid, has been the most widely used polymer for bioprinting applications.[10] Ideally, a bioink should exhibit shear-thinning rheology along with substantial yield stress to enable extrusion and further rapid gelation postbioprinting.[13] Alginate had earlier been used for drug delivery and tissue engineering because of its bioinertness and

[a)]Address all correspondence to this author.
e-mail: pd@chest.iiests.ac.in, contactpallab@gmail.com
DOI: 10.1557/jmr.2018.202

 © Materials Research Society 2018

https://doi.org/10.1557/jmr.2018.202 Published online by Cambridge University Press

low-cost, but its application in bioprinting is largely driven by its ability to undergo fast gelation under exposure to Ca^{2+} ions under physiological pH and temperature conditions. The rapid gelation properties of alginate were extremely suitable for fabricating cell-laden tissue constructs using different bioprinting modalities.[10] However, rapid instantaneous gelation can also cause nozzle clogging and printing inhomogenities. Conversely, delayed crosslinking leads to shape distortions and reduces fidelity of bioprinted constructs. Thus concentration optimization of crosslinker and alginate has been attempted in many reports. Additionally, the strong hydrophilic nature of alginate allows only limited cell–material interactions causing cells to be present in an immobilized state.[14] Inadequate degradation of alginate is also a constraint for effective cell proliferation and differentiation in 3D scaffolds.[15] To overcome these limitations, low alginate concentrations have been used to obtain higher cell functionalities. However, lowering the concentration compromises mechanical robustness of constructs. Other approaches to improve the bioprintability of alginate involve chemical modification of alginates to oxidized alginate[16] or RGD-conjugation of alginate,[15] and blending with other polymers.[17] However, these methods essentially contribute a different chemical scheme reducing the physiological conditions in which alginate bioprinting would be eventually performed. For example, oxidized alginate bioinks are shown to require higher Ca^{2+} ion concentrations to induce gelation, which may be deleterious to certain cell types.[18] From the precluding information, it can be expected that a cell responsive material, which can be homogenously blended with alginate and possess optimum rheological properties and gelation time properties, may confer an ideal bioink for bioprinting of cell laden constructs.

Honey, a carbohydrate-rich multicomponent natural product, has well documented wound healing properties in traditional medicine and continues to obtain favorable dermatological opinion as an efficacious agent for healing of various cutaneous wounds.[19–23] Based on the favorable biological properties, honey has been blended with several polymers like chitosan, poly(vinyl alcohol), gelatin, alginate, and poly(ethelene terephthalate) to prepare matrices for tissue engineering and wound regeneration.[21,24,25] Such honey-based matrices have been fabricated in the form of nanofibers, films, and hydrogels.[21,26] Notwithstanding the beneficial effects of honey-based matrices and wound dressing systems, to the best of our survey, honey-based 3D-printed scaffolds have not been yet reported in the literature. Therefore, the present investigation is conducted with the hypothesis that honey as a bioink component can improve the biological properties of alginate-based bioprinted constructs. Moreover, honey is shown to have dose-dependent effects on various biological responses and is even active at low blending ratio with the polymers.[27] Therefore, the present study also examines for the first time the effect of different low-concentrations of honey blended with alginate as bioink on the cellular biocompatibility of the bioprinted constructs. Importantly, honey is a viscous solution and can be blended with alginate. This propels interest to examine if honey-blended alginate can be used as a bioink for bioprinting applications. Viscosity of honey is expected not to compromise the viscosity of alginate solutions required for bioprinting while its activity at low additions is not expected to significantly increase the Ca^{2+} ion concentration for crosslinking. Thus a bioactive construct can be generated. With this objective, the present investigation reports the effect of honey blending on physicochemical properties of alginate bioinks, followed by bioprintability studies and evaluation of shape fidelity and mechanical properties of bioprinted constructs. It was assumed that honey blending will alter the rheological properties of alginate; therefore, the bioink formulation containing honey that would increase cell responsiveness without remarkable compromise in other extrusion printing properties was optimized and is reported. The biological responsiveness of constructs is evaluated by culture of fibroblast cells.

II. MATERIALS AND METHODS

A. Preparation of alginate:honey bioinks

Alginic acid sodium salt from brown algae (Alginate, A2033-250G, Lot # SLBQ3067V with Pcode: 1002311747) was purchased from Sigma-Aldrich (St. Louis, Missouri) and commercial honey (Dabur, Ghaziabad, India, Batch No. BD0793) was purchased from reputed commercial manufacturer in India. Various concentrations of alginate:honey (AH) solutions were prepared, in which the concentration of alginate was fixed at 5% (w/v) in ASTM Type III Grade water (Wasserlab, Navarra, Spain) and the concentration of the honey was varied in the range 1–5% (w/w) of solution for AH solutions as summarized in Table I. All AH solutions were prepared freshly and stirred in a mechanical stirrer for 24 h prior to use in any experiment.

TABLE I. Summary of different AH bioink formulations along with their physicochemical properties.

Sample	Composition (% w/v)		pH	Conductivity (μS)	Viscosity (Pa s)	Surface tension (N/m)
	Alginate	Honey				
A5H0	5	0	7.5	28.4 ± 5.5	9.7 ± 0.0	71.6 ± 1.5
A5H1	5	1	7.4	21.0 ± 2.2	6.2 ± 1.1	66.0 ± 0.1
A5H2	5	2	7.4	19.3 ± 1.9	6.1 ± 0.0	58.0 ± 0.0
A5H5	5	5	7.3	17.6 ± 2.3	6.0 ± 0.0	53.2 ± 2.1
A5H10	5	10	7.1	12.5 ± 2.1	5.5 ± 0.1	47.3 ± 1.2

https://doi.org/10.1557/jmr.2018.202 Published online by Cambridge University Press

B. Physicochemical characterization of AH inks

pH and conductivity of bioinks were recorded in a Thermo Oakton meter at 25 °C. Viscosity of inks was measured using a Lamy Rheology viscometer (Champagne au Mont d'Or, France) at a temperature of 25 °C. Spindle L-4 was used to measure the viscosity at a constant torque of 6 rpm for 60 s. Surface tension of bioinks was measured by surface tensiometer SURFTENS 4.5 (OEG GmbH, Hessisch Oldendorf, Germany) using a glass slide as the substrate. The inverted glass vial method was performed to determine the gelation time of the inks. AH solutions were mixed with 1 mL 0.5 M $CaCl_2$ and capped tightly with parafilm in a 25 mL glass vial. The glass vials were inverted every 1 min and held for 20 s after addition of $CaCl_2$ to AH blend solutions to measure the gelation time of the bioinks, recorded as the time point when the inks stopped flowing.

C. Extrusion bioprinter

Our custom bio 3D printer is a 4-axis machine with *X*, *Y*, *Z*, and syringe pump extruder control. The *X* and *Y* axes are controlled by a stepper motor driven on linear bearings while the *Z*-axis is driven by a lead screw. The syringe pump is controlled by a geared stepper motor that steps up the torque and increases extrusion pressure. There is a provision for heated bed as well so that the Petridish can be kept at a specified temperature. A 32-bit SAM controller, with software orthogonal compensation and automatic bed leveling, ensures high precision of the prints. We used Cura, open-source slicing software, to slice our 3D models and Pronterface to issue G-Codes to control our bioprinter.

D. Design of scaffolds

Lattice structures of dimensions of 34 × 34 mm (*X*, *Y*) were designed using Sketchup software in .stl format (Trimble Inc., Sunnyvale, California). The solid object was then sliced by CURA™ version 15.04.4. By changing the fill density of the solid object from 100% to 23%, a mesh-type structure was created. The desired mesh structure, represented in Fig. 1, saved in G-Code format and is uploaded in the 3D printer for printing.

E. Extrusion printing of AH inks

The AH ink were then loaded into a printer-compatible syringe. Printing was performed with a print speed of 50 mm/s and a nozzle diameter of 3 mm at 25 °C temperature. Lattice structures were printed, using a point-to-point strategy to print every other dot, which is a result of a printing design with dimensions of 34 × 34 mm (*X*, *Y*). AH inks were extruded on a glass Petridish containing 0.5 M $CaCl_2$ solution. Postprinting, lattice scaffolds were washed with ethanol (95%, Himedia, Mumbai, India) thrice for 10 min each and dried in a vacuum oven at 40 °C.

F. Characterization of AH-printed scaffolds

Macroscopic images were acquired through a Nikon Digital camera (NIKON DS-Fi1c, Nikon, Tokyo, Japan).

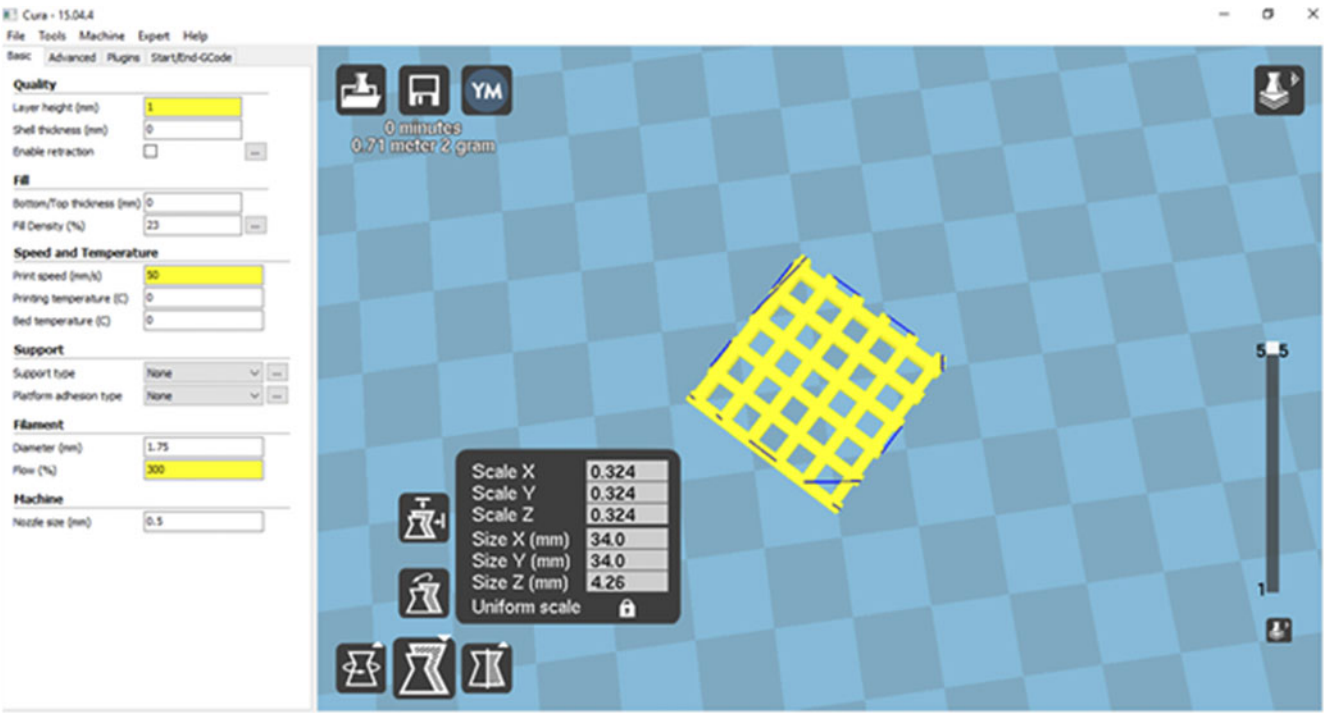


FIG. 1. Lattice scaffolds designed by CURA™ software.

https://doi.org/10.1557/jmr.2018.202 Published online by Cambridge University Press

Three images were acquired for each sample at a magnification of 10×. The calculation of the strut length (SL), pore areas (PA), and perimeter (P) were performed by AxioVision SE64 Rel. 4.9.1 software (Carl Zeiss, Jena, Germany). Chemical characterization was performed with Fourier transform infrared spectroscopy (Jasco, Tokyo, Japan FT/IR-4600) in the ATR mode in the range 4000–400 cm^{-1}.

G. Printability analysis

The quantitative analysis of post-3D printing structures is still undergoing standardization and has often been subjected to trial and error. However, over the years, a number of mathematical models as well as computational methods have been developed to semiquantify the printability of the post-3D printed structures.[28,29] One of the most useful metrics has been proposed by Oyang et al.[30–32] to study the printability of 3D-printed structures by applying mathematical formulae as represented in the following equations.

$$C = \frac{4\pi A}{P^2} \quad , \tag{1}$$

$$\mathrm{Pr} = \frac{\pi}{4C} \quad . \tag{2}$$

The mathematical model is based on the principle that circularity (C) is highest in case of circles, so C is equal to 1 for circles. Therefore, for Eq. (1), the closer the values are to 1, the more circular they are. Furthermore, printability (Pr) is defined by using Eq. (2), which is based on a square. It is stated that for ideal Pr status, the interconnected channels of the constructs would demonstrate a square shape, with a Pr value of 1. The area and the perimeter of the interconnected channels of the constructs was calculated using AxioVision SE64 Rel. 4.9.1 software. The C values were then calculated for various samples and further used to analyze the Pr values. The values of C and Pr for the various samples along with the sample codes are tabulated in Table II. For each group, five samples were fabricated for measurements.

The study used a blend solution with honey content ranging from 0 to 5% and alginate content 5%. The C and Pr values for the various samples were calculated and further used for the printability analysis of the samples. The mathematical model used states that the Pr value of 1 would give the perfect printability status. The samples were therefore semiquantified on the basis of how closer the values are to 1. The accuracy of the printed scaffolds were also determined based on the differences between the input and the output scaffold dimensions. Each scaffold contains 25 pores. Comparison of the printed area with the designed area was done to get percentage printing accuracy.[33] A_0 (756 mm^2) is the input area and A_d (X mm^2) is the output area of the scaffolds. Percentage printing analysis is reported based on measurements of five scaffolds for each group.

$$\text{Accuracy of printing } (\%) = \left[1 - \frac{|A_d - A_0|}{A_0}\right] \times 100 \quad . \tag{3}$$

H. Mechanical characterization of AH scaffolds

The uniaxial tensile property was measured by using the universal testing machine (Tinius Olsen 5 KT, Tinius Olsen, U.K.). Sample dimensions of 34 × 34 × 5 mm were used for the test, and tests were performed at a tensile speed of 0.1 mm/min with a load cell of 125 N. The samples were gripped with clip-type sample holder with a gripping zone length of 10 mm. Three samples for scaffold (each bioink formulations) were tested. Before testing each sample, the specimens were preconditioned for ten preconditioning cycles up to 10% strain and observed to see if the structure of the samples were consistent. The nominal stress at which the samples failed was taken as the ultimate stress of the scaffolds.

I. Release of honey from the scaffolds

To quantify the release of honey from the printed A5H5 scaffolds (1.5 × 1.5 cm), the samples were incubated in 10 mL of sterile phosphate buffered saline (PBS) and a supernatant was obtained immediately after incubation and thereafter on 2 and 4 days of incubation. Corresponding scaffolds without honey (A5H0) were treated as blank for respective time points. After incubation for the designated time points, the releasate from the scaffolds was assayed for glucose as an indicator of honey release, following the procedure given in Ref. 34. Additionally, to determine the functionality of scaffolds

TABLE II. Geometrical and printability analysis of scaffold printed with different honey alginate bioink formulations.

	Strut diameter (mm)	Pore area (mm^2)	Perimeter (mm)	Circularity	Printability	Printing accuracy (%)
A5H0	0.11 ± 0.02	3.87 ± 1.43	7.39 ± 0.83	0.88	0.88	89 ± 0.56
A5H1	0.14 ± 0.02	4.05 ± 0.64	8.29 ± 0.48	0.76	1.01	84 ± 1.54
A5H2	0.16 ± 0.02	5.67 ± 1.64	10.68 ± 1.32	0.62	1.26	81 ± 0.78
A5H5	0.20 ± 0.00	8.32 ± 1.60	13.81 ± 2.46	0.54	1.44	76 ± 0.43

Intended pore area: 15 mm^2; intended strut diameter 2.3 mm.

https://doi.org/10.1557/jmr.2018.202 Published online by Cambridge University Press

with time, 2,2-diphenyl-1-picrylhydrazyl (DPPH) activity was measured at each time point following the procedure published elsewhere.[35] The A5H0 scaffolds were treated as blanks for the different time points of measurement.

J. Cell culture study

The scaffolds (~10 mm × 10 mm, 100 μm thickness) were assessed for adhesion and proliferation of 3T3 fibroblast cells. Cells were cultured in 10% fetal bovine serum-supplemented Dulbecco's modified Eagle's medium (DMEM) (Gibco, Carlsbad, California) supplemented with 1% (of 100×) antibiotic (penicillin–streptomycin). The cells were harvested by trypsinization from T25 flask and centrifuged at 1500 rpm for 5 min, and resuspended in complete DMEM to obtain a concentration of 2×10^6 cells per mL. The cells were further seeded on sterilized scaffolds at the concentration of 10^4 cells per mL and incubated (37 °C, 5% CO_2). Adhesion was analyzed using measuring cell viability on day 1 by 3-[4,5-dimethylthiazol-2-yl]-2,5-diphenyltetrazolium bromide (MTT) assay within a 12-well plate. After culturing cells on the scaffolds, the cells were trypsinized, and the MTT reagent was added to each sample and incubated for 4 h. Formazan crystals formed were solubilized in buffer, and the product was transferred into a 96-well-plate. Absorbance at 595 nm was recorded using a Multi-Scan Go (Thermo Fisher, Vantaa, Finland), and the viability was further calculated. To evaluate cell proliferation, the same assay procedure was repeated on day 3. The cell viability normalized to the initial solid surface area of each sample was calculated. Cell viability represented is relative to the absorbance value recorded on day 1 of the control tissue culture polystyrene (considered as 1). All values are expressed as mean ± standard deviation of at least three experiments with different experiments and compared using ANOVA with Bonferroni as a post hoc test. Values of $P < 0.05$ were considered as significant.

K. Microscopy of cell-scaffold constructs

Cultured-cell staining was performed on the constructs on day 5. The cells were fixed in 3.7% formaldehyde for 10 min followed by permeabilization at 4 °C for 5 min in a buffer solution (50 mM NaCl, 150 mM sucrose, 3 mM $MgCl_2$, 50 mM Tris base, 0.5% Triton X-100). Incubation of constructs for 60 min was further performed at 37 °C with blocking buffer [1% bovine serum albumin (BSA), 0.1% Tween-20, 0.02% sodium azide in PBS]. After washing in PBS, the samples were incubated for 60 min at 37 °C with rhodamine-phalloidin solution [diluted 1:200 (Invitrogen, Carlsbad, California)] and 4′,6-diamidine-2′-phenylindole dihydrochloride (DAPI) (Sigma-Aldrich, Saint Louis, Missouri). The samples were observed under a Nikon inverted fluorescence microscope (ECLIPSE TE 300, Nikon, Tokyo, Japan).

III. RESULTS AND DISCUSSION

A. Physicochemical properties of AH inks

Extrusion 3D printing with biopolymers and 3D bioprinting (combined referred to as bioprinting in this paper) has emerged as promising tools for tissue engineering and drug discovery. The ability to deposit biomaterials and cells simultaneously allows for more precise reconstruction of cellular niche and better cell–cell and cell–matrix interactions. Amongst other bioprinting modalities, extrusion bioprinting is highly scalable and appropriate for obtaining mechanically robust scaffolds. However, one of the challenges that remain to be overcome for full realization of benefits of the extrusion bioprinting technique is the development of suitable biopolymer-based bioinks. Developing such bioinks has remained challenging because of several reasons. First, biopolymer should be able to maintain physiological pH in solution to incorporate living cells (one of the principal reasons in favor of alginate-based inks). Second, the polymer solutions should have shear thinning properties such that it is easily extruded without clogging during the printing process but regain their structural consistency immediately after printing; this ensures that bioprinted constructs resemble the designed structure as well as are solidified rapidly to allow for supporting the next layers. To achieve rapid solidification, crosslinking is often required and preferably conducted under physiological temperature and pH to cause minimal damage to cellular bioink components. Furthermore, a bioink is required to possess adequate biocompatibility and cell adhesion properties for cells to adhere to biomaterial postprinting. Alginate, though qualifies most of the physicochemical properties required for bioprinting, suffers from poor cell adhesion properties, requiring efforts to improve cell adhesion of alginate without compromising on the physicochemical attributes. To date, a number of studies have used different concentrations of alginate ranging from 2 to 4% for fabrication of optimized 3D-printed scaffolds.[11] In the present study, however, 5% alginate was mixed with low concentrations of honey (0, 1, 2, and 5%) to investigate the potential of AH formulations as potential bioinks. The addition of honey causes change in both physiological as well as biological properties of the pure alginate bioinks.

Initially, the solution properties of AH formulations were compared. The viscosity values measured were 9.7 ± 0.1, 6.2 ± 1.0, 6.1 ± 0.0, 6.0 ± 0.0, and 5.5 ± 0.1 Pa s. Bioprinting with bioinks of similar viscosity ranges have been performed by other researchers.[36,37] It is seen that as the concentration of the honey is increased, viscosity of AH solutions decreases. This is due to less viscosity of honey compared to alginate solution and further penetration of honey components in the alginate chains, which significantly reduce polymer chain

https://doi.org/10.1557/jmr.2018.202 Published online by Cambridge University Press

entanglements. However, the range of viscosity recommended suitable for bioprinting is 0.3–30 Pa s,[36] and all of the formulations tested in the present work possess the viscosity in this range. Moreover, this viscosity range is maintained with a higher alginate concentration (5% w/v) compared to 2–4% reported elsewhere, which may be advantageous for obtaining more mechanically robust constructs. The results of the physicochemical properties are summarized in Table I. Addition of honey at various concentrations affected the time required for gelation of the alginate solutions. The gelation time varied in the values of 1, 2, 4, and 6 min as the concentration of the honey in alginate solution was increased. This may be favorable for reducing clogging events using high alginate concentrations provided structural fidelity is retained. Essence of alginate for bioprinting applications has been drawn from ease of gelation at physiological conditions, most commonly by the diffusion of gelling (Ca^{2+}) ions.[38] However, as also encountered in production of microbeads, the rapid gelation limits diffusion of Ca^{2+} into the interior gel network, causing distortions in producing more complex-shaped structures as well as causing inhomegenously crosslinked gels, which result in erratic degradation time of alginate hydrogels. One of the most common approaches to improve both erratic degradation behavior as well as cell responsiveness of bioprinted alginate scaffolds has been to blend with gelatin as one of the bioink formulation ingredients. RGD sequences of gelatin are supposed to improve cell adhesion.[38] However, gelatin-alginate blend bioink shifts the gelation conditions like temperature to nonphysiological range (11 °C in 2% alginate-gelatin blends as reported in Ref. 39), thus diminishing their utility for cell-laden bioprinting. Thus, the low honey loaded AH gels with delayed gelation times under more physiologically acceptable conditions can be advantageous, provided shape fidelity is also maintained. The results indicate that the decrease in viscosity can improve clogging properties while honey incorporation can allow extrusion with 5% alginate solutions, which compared to general 3–4% w/v solutions reported in the literature, can provide constructs with better mechanical properties.

B. Structural fidelity of AH-printed scaffolds

The uniformity of shapes of the bioprinted constructs after extrusion from the nozzle was analyzed and it was seen that honey addition affected bioprinted shapes as suspected from the increase in gelation times. Compositions A5H0, A5H1, A5H2, and A5H5 were printed with properly defined shapes. By contrast, when compositions with higher than 5% honey was used, the structure was not retained and flowed readily at the given pressures. Thus, this concentration was not appropriate for printing (images not shown). In a previous report, molecular weight and concentration of alginate hydrogels were shown to influence bioprinting shapes.[40] Similarly, we found that bioinks containing larger content of honey did not show sufficient printability for an effective 3D printing process. As can be seen from Table II and Figs. 2(a)–2(e), the strut size increased and the pore area decreased as honey concentration was increased. This can be attributed to the decrease in viscosity in consonance with effects observed with gelatin alginate bioinks.[39] As already discussed, bioinks require sufficient viscosity to maintain their 3D porous structure during and after printing. For these reasons, bioink compositions up to 5% honey were chosen to investigate mechanical and cellular behaviors in 3D-printed porous scaffolds.

Apart from determination of deviation of strut width and pore diameters, circularity and printability parameters were studied to obtain a more robust evaluation of print fidelity. This is based on the studies of Oyang et al. who proposed that square holes will be formed under proper gelation conditions, whereas layer fusion creating circular pores will be formed under the liquid-like inadequate gelation condition.[31] It is observed that with increasing concentration of honey, the values of C are decreasing and the values of Pr are increasing. On the contrary, as shown in Fig. 2(f), it is clear that a very high value of Pr also does not give good printability. For the sample to have a good printability, the Pr value should be close to 1.

It is seen from the data that pore size decreased first as the concentration of the honey was increased from 0 to 2% but further decreased as the concentration of honey was increased to 5%. The strut diameter increases with the increasing concentration of honey, which corresponds to a decrease in viscosity of the solutions. The stability and print fidelity of the samples were analyzed with the help of the mathematical formula as described earlier. By this parameter, formulations A5H1 and A5H2 can be considered to be providing most acceptable bioprinted scaffolds. The values of Pr which are close to 1 show that the filaments are formed smoothly and thus the samples show stable structures. Figure 2(f) shows the shape of pores for values of Pr less than, equal to, and more than one. Accuracy of the printed scaffolds was measured, and it was seen that increasing the concentration of honey decreases the accuracy. For A5, A5H1, A5H2, A5H5, and A5H10, the percentage accuracy was 89%, 84%, 81%, 76%, and 69%, respectively. The printing accuracy of the 3 × 3 grid was measured by Giuseppe et al.,[41] who also found higher accuracies for structures with high polymer concentrations.

From this analysis, it was evident that for clogging-free printing, A5 is the most suitable ink formulation though the structure was not able to maintain integrity. Bioink formulation A5H1 and A5H2 resulted in stable

https://doi.org/10.1557/jmr.2018.202 Published online by Cambridge University Press

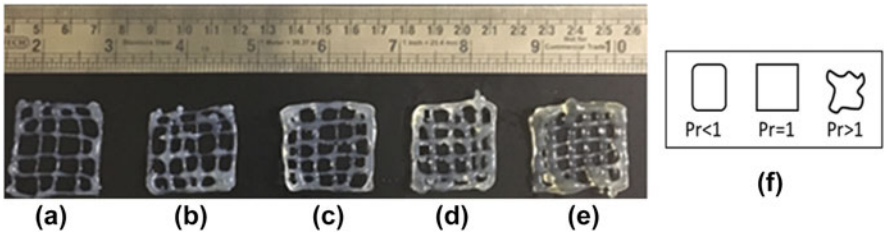


FIG. 2. Optical images of the printed honey-alginate lattice scaffolds: (a) A5H0, (b) A5H1, (c) A5H2, (d) A5H5, (e) A5H10, and (f) geometric description of the printability parameter as proposed by Refs. 30–32.

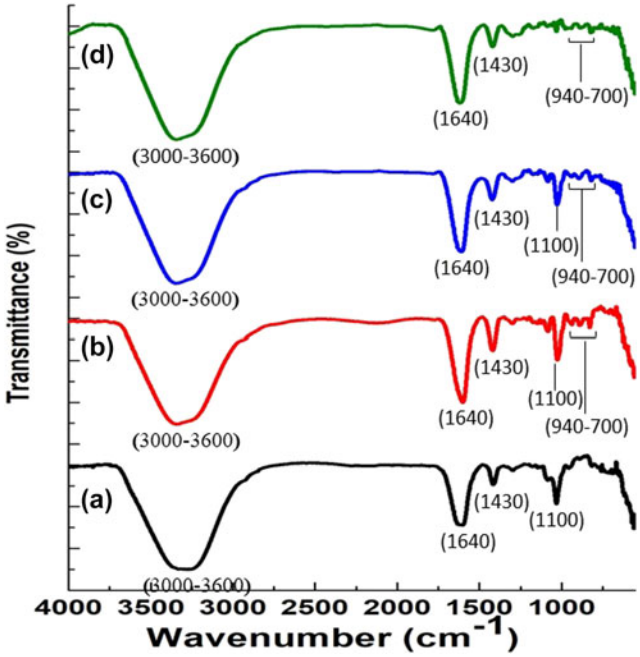


FIG. 3. FTIR Spectrum of printed AH lattice scaffolds: (a) A5H0, (b) A5H1, (c) A5H2, and (d) A5H5.

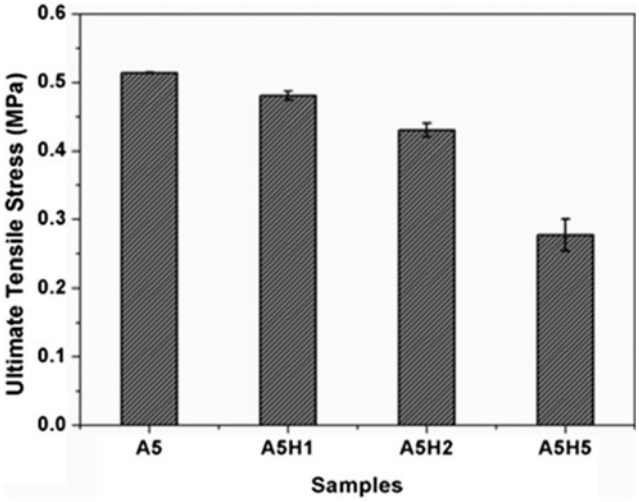


FIG. 4. Mechanical properties of printed honey alginate scaffolds.

structures. The best construct fidelity was obtained with A5H1 and A5H2 formulations.

C. Characterization of printed AH scaffolds

Figure 3 shows the FTIR spectra of the sodium alginate with concentration 5% and varying honey concentrations of 0, 1, 2, and 5%. Stretching vibrations of O–H bonds of alginate and honey appeared in the range of 3000–3600 cm^{-1}. Bands observed in 1640 and 1430 cm^{-1} were attributed to asymmetric and symmetric stretching vibrations of carboxylate salt ion, respectively, present in algiante. The bands at 1100 are attributed to the C–O stretching vibration of pyranosyl ring and the C–O stretching with contributions from C–C–H and C–O–H deformation. The vibrations found in the region of 940–700 cm^{-1} correspond to the anomeric regions of honey.

Figure 4 shows the mechanical strength of the printed scaffolds. The results show that there is a decrease in tensile strength with increasing concentration of honey. For the samples A5H0, A5H1, A5H2, and A5H5, corresponding values obtained were 510 kPa, 480 kPa, 440 kPa, and 280 kPa, respectively. However, such alterations in mechanical properties can be used to modulate the concentration of honey to get the tissue-specific tensile strengths and promote tissue-specific differentiation of stem cells.[42] Elsewhere, the modulus of 5% alginate crosslinked with 1 M $CaCl_2$ has been found to be 250 kPa[43] while recent reports on alginate/poly(vinyl alcohol) bioprinted scaffolds also show similar mechanical behavior.[17] Glucose release has been a method adopted for understanding the release of honey from scaffolds.[34,44,45] The release of glucose and the antioxidant potential of the scaffolds were measured at various time points as shown in Fig. 5. The scaffolds showed progressive increase in glucose starting from day 0 to day 4. No release was obtained on day 0, i.e., at the start of incubation, whereas on day 2 and day 4, the corresponding values measured were 63 and 148 mg/dL, respectively, indicating that the rate of release of glucose was increasing with incubation time. On the other hand, DPPH activity showed the values of 4.5% and 6.5%, respectively, on day 2 and day 4, indicating that maximum release of antioxidant components were

https://doi.org/10.1557/jmr.2018.202 Published online by Cambridge University Press

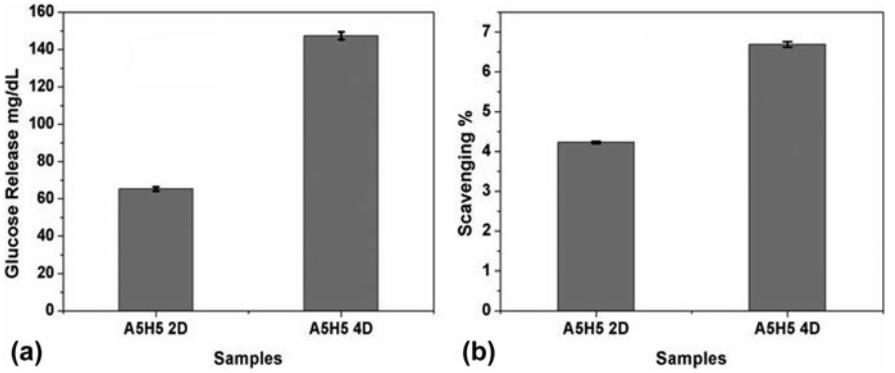


FIG. 5. Release of honey constituents over time estimated by (a) glucose release from A5H5 bioprinted scaffolds in PBS on day 2 and day 4 of incubation and (b) antioxidants activity on similar days.

accomplished initially. Previous studies have also reported a glucose release of around 0.5 mg/mL from different types of honey-based scaffolds like cryogels and electrospun nanofibers.

D. Cellular compatibility of AH scaffolds

Bioinks were evaluated for their biocompatibility by culture of fibroblast cells on the printed scaffolds. Cell viability on day 1 on A5H1, A5H2, and A5H5 scaffolds were measured and found to be significantly different from A5H0, as depicted in Fig. 6 ($P < 0.05$). This shows that honey can also increase the initial cell adhesion of alginate scaffolds. Although increase in cell viability due to honey incorporation in tissue engineering matrices has been reported earlier by several studies, the direct mechanism is still unknown.[46] However, some reports show that honey contains some proteins like Down syndrome cell adhesion molecule-like protein (Dscam2) with cell adhesion properties in vitro.[47] After 3 days of culture cell, it was seen that viable cell numbers increased in all the scaffolds, with the highest increase observed in A5H2. Day 3 cell viability on A5H2 was significantly higher than A5H1 and A5H0. However, no significant difference between A5H2 and A5H5 was observed. The results show that bioinks with honey at 2 and 5% concentrations showed the highest cell proliferation, with no significant differences between them.

Figures 7(a)–7(d) show the fibroblast cells cultured on different scaffolds stained with rhodamine phalloidin after 5 days of incubation. As can be seen from the figure, the cells cultured on A5H2 are higher in number compared to other groups. Except A5H0, the cells were shown to be in a more spread-out morphology in the other groups. This result indicates that cell–cell interactions are stronger than cell–material interactions on pure alginate, which gradually reverses due to incorporation of honey. In the literature, the effect of honey concentrations in modulating cell viability and proliferation has been reported and ascribed to differential

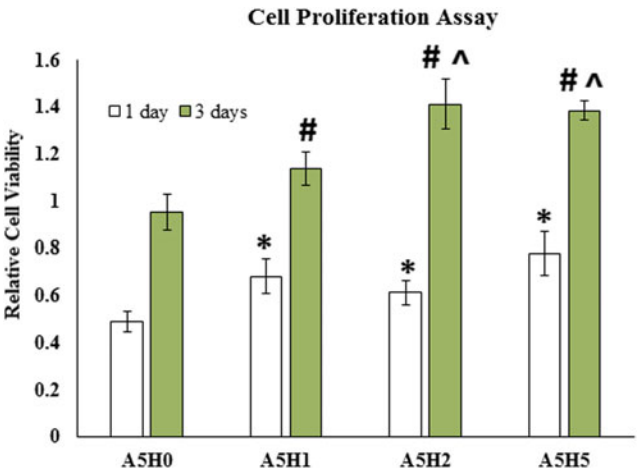


FIG. 6. Cell viability of honey alginate scaffolds on day 1 and day 3 of fibroblast cell culture expressed relative to viability of tissue culture polystyrene (day 1). *, #, and ^ denote statistically significant ($P < 0.05$) difference with A5H0 day 1, A5H0 day 3, and A5H1 day 3, respectively. The difference between viability of day 3 and day 1 for all the groups was statistically significant.

expression of different proliferation factors such as p63. Elsewhere, the positive cellular and in vivo responses of honey in wound healing have been attributed to epithelial to mesenchymal transitions,[48] and anti-inflammatory[49] and immune-modulatory caused by honey interventions.[23] Several bioinks are now under development for extrusion-based bioprinting including alginate, GelMA, agarose, collagen, fibrin, silk, poly(ethylene glycol), and hyaluronic acid. A bioink must possess a suitable biofabrication window, which satisfies the contradictions between rheology and cell compatibility of polymers used. While low polymer-loaded bioinks are beneficial for cell proliferation and differentiation, bioinks with polymer sols at higher concentrations are required to confer suitable rheology to bioinks as well as mechanical properties of bioprinted scaffolds. High polymer concentrations can also require high pressures causing shear-induced (e.g., >60 kPa) cell deaths.[50,51]

https://doi.org/10.1557/jmr.2018.202 Published online by Cambridge University Press

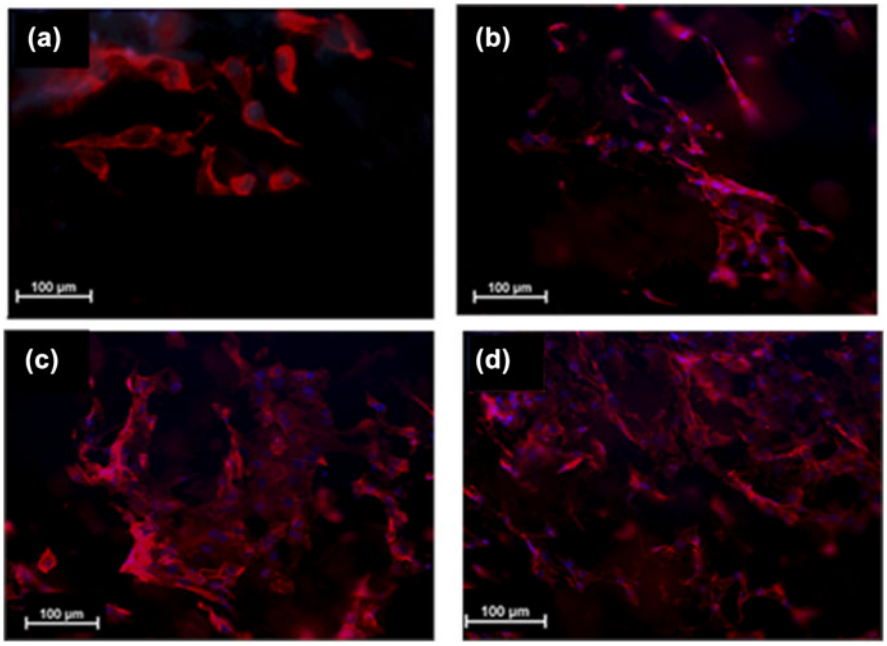


FIG. 7. Fluorescence DAPI/phalloidin rhodamine stained images of fibroblast cells seeded on printed scaffolds after 5 days of culture in (a) A5H0, (b) A5H1, (c) A5H2, and (d) A5H5.

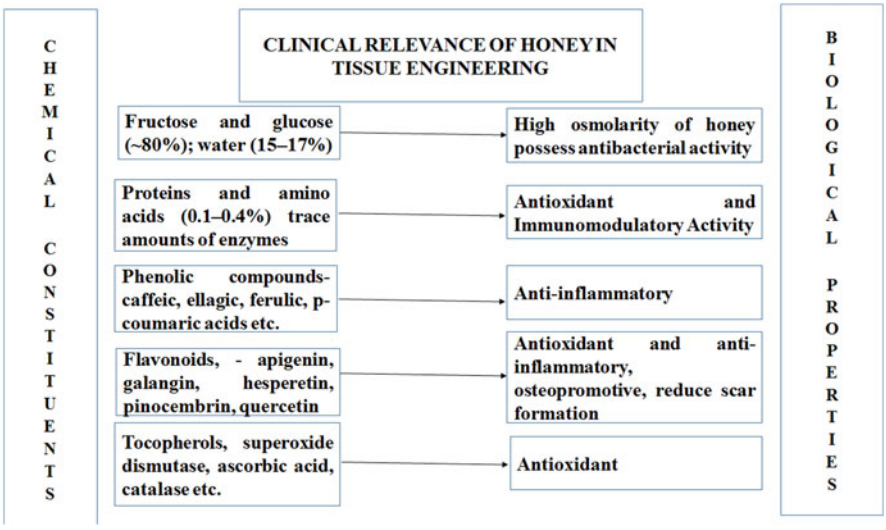


FIG. 8. Relation between chemical constituents of honey and their biological implications for tissue engineering.

At present, clinical conditions of full-thickness skin wounds and extensive burns remain refractory to complete regeneration, whereas autologous split-thickness grafting continues to be the most acceptable solution. However, in large wound areas, the availability of adequate autologous donor tissue is limited.[52] The traditional tissue engineering modalities do not allow for simultaneous fabrication of cells and biomaterials for mimicking the layer-specific heterogeneous composition of skin tissue. Moreover, many large area wounds have irregular shapes and off-the-shelf bandages are not often sufficient to meet the requirements of clinical burn surgeries. 3D bioprinting has emerged as a potential solution to overcome the limitations of current tissue engineering, wherein one study claiming has obtained 100 cm^2 of bioprinted skin tissue under 35 min.[7] In situ clinical 3D bioprinting thus holds great clinical potential. However, material additives for such clinical applications should not have any toxicity and be readily available. In this respect, the use of an easily available viscous natural material honey which can promote cell adhesion and proliferation along with possessing anti-inflammatory,

https://doi.org/10.1557/jmr.2018.202 Published online by Cambridge University Press

anti-bacterial, anti-oxidant, anti-bacterial, and pro-angiogenic attributes (see Fig. 8),[21,35,53] when blended at low concentrations within a polymer bioink formulation without affecting the rheological properties to a great extent, can be a promising material for bioprinting at physiological conditions.

IV. CONCLUSIONS

We presented results of an investigation on honey-blended alginate bioinks for obtaining in situ bioprinted skin tissue engineering constructs. The 1–2% honey ratio has provided bioprinted scaffolds with improved cell proliferation without any remarkable decrease in printability. It is observed that viscosity of bioinks can be the important physicochemical control parameter for predicting bioprinting accuracies. A small 10% reduction in mechanical strength is evident, which may be accepted for certain soft tissue engineering applications given the improved biological response. There is an increase in cell viability on 2% honey loaded bioprinted scaffolds. Further optimization within this range can potentially facilitate the fabrication of different complex human skin structures. However, in the present report, the effect of different bioprinting parameters like extrusion speed and pressure to improve accuracy and resolution of constructs have not been studied, which will be required in future for clinical translations. Additionally, the fabrication of cell-laden matrices with honey as the bioink component at exact physiological temperatures would be interesting to observe as honey contains several antioxidants to mitigate cell death during bioprinting. Considering the advantages of honey as a potential wound healing agent, this approach may be a facile method for obtaining bioprinted scaffolds in the clinic.

ACKNOWLEDGMENTS

The authors acknowledge financial support from Department of Science and Technology, Govt. of India vide DST/IFA/12/LSBM/48 to PD and IIEST institute fellowship support to SD.

REFERENCES

1. S. Bose, D. Ke, H. Sahasrabudhe, and A. Bandyopadhyay: Additive manufacturing of biomaterials. *Prog. Mater. Sci.* **93**, 45 (2018).
2. I.T. Ozbolat, W. Pemg, and V. Ozbolat: Application areas of 3D bioprinting. *Drug Discov. Today* **21**, 1257 (2017).
3. P.F. Egan, V.C. Gonella, M. Engensperger, S.J. Ferguson, and K. Shea: Computationally designed lattices with tuned properties for tissue engineering using 3D printing. *PLoS One* **12**, e0182902 (2017).
4. W. Peng, P. Datta, B. Ayan, V. Ozbolat, D. Sosnoski, and I.T. Ozbolat: 3D bioprinting for drug discovery and development in pharmaceutics. *Acta Biomater.* **57**, 26 (2017).
5. L. Ning and X. Chen: A brief review of extrusion-based tissue scaffold bio-printing. *Biotechnol. J.* **12**, 1600671 (2017).
6. I.T. Ozbolat and M. Hospodiuk: Current advances and future perspectives in extrusion-based bioprinting. *Biomaterials* **76**, 321 (2016).
7. N. Cubo, M. Garcia, J.F. Cañizo, D. Velasco, and J.L. Jorcano: 3D bioprinting of functional human skin: Production and in vivo analysis. *Biofabrication* **9** (2016).
8. S. Duchi, C. Onofrillo, C.D.O. Connell, R. Blanchard, A.F. Quigle, R.M.I. Kapsa, P. Peter, G. Wallace, C. Di Bella, and P.F.M. Choong: Handheld co-axial bioprinting: Application to in situ surgical cartilage repair. *Sci. Rep.* **7**, 5837 (2017).
9. K.W. Binder, W. Zhao, T. Aboushwareb, D. Dice, A. Atala, and J.J. Yoo: In situ bioprinting of the skin for burns. *J. Am. Coll. Surg.* **211**, S76 (2010).
10. M. Hospodiuk, M. Dey, D. Sosnoski, and I.T. Ozbolat: The bioink: A comprehensive review on bioprintable materials. *Biotechnol. Adv.* **35**, 217 (2017).
11. S.K. Williams and J.B. Hoying: Bioinks for bioprinting. In *Bioprinting in Regenerative Medicine*, K. Turksen, ed. (Springer International Publishing, Cham, 2015); pp. 1–31.
12. K. Hölzl, S. Lin, L. Tytgat, S. Van Vlierberghe, L. Gu, and A. Ovsianikov: Bioink properties before, during and after 3D bioprinting. *Biofabrication* **8**, 032002 (2016).
13. A. Abbadessa, M.M. Blokzijl, V.H.M. Mouser, P. Marica, J. Malda, W.E. Hennink, and T. Vermonden: A thermo-responsive and photo-polymerizable chondroitin sulfate-based hydrogel for 3D printing applications. *Carbohydr. Polym.* **149**, 163 (2016).
14. T. Billiet, M. Vandenhaute, J. Schelfhout, S. Vlierberghe, and P. Dubruel: A review of trends and limitations in hydrogel-rapid prototyping for tissue engineering. *Biomaterials* **33**, 6020–6041 (2012).
15. Z. Wu, X. Su, Y. Xu, B. Kong, W. Sun, and S. Mi: Bioprinting three-dimensional cell-laden tissue constructs with controllable degradation. *Sci. Rep.* **6**, 24474 (2016).
16. J. Jia, D.J. Richards, S. Pollard, Y. Tan, J. Rodriguez, R.P. Visconti, T.C. Trusk, M.J. Yost, H. Yao, R.R. Markwald, and Y. Mei: Engineering alginate as bioink for bioprinting. *Acta Biomater.* **10**, 4323 (2014).
17. Y. Luo, G. Luo, M. Gelinsky, P. Huang, and C. Ruan: 3D bioprinting scaffold using alginate/polyvinyl alcohol bioinks. *Mater. Lett.* **189**, 295 (2017).
18. L.Q. Wan, J. Jiang, D.E. Arnold, X.E. Guo, H.H. Lu, and V.C. Mow: Calcium concentration effects on the mechanical and biochemical properties of chondrocyte-alginate constructs. *Cell. Mol. Bioeng.* **1**, 93 (2008).
19. L. Vandamme, A. Heyneman, H. Hoeksema, J. Verbelen, and S. Monstrey: Honey in modern wound care: A systematic review. *Burns* **39**, 1514 (2013).
20. S.K. Saikaly and A. Khachemoune: Honey and wound healing: An update. *Am. J. Clin. Dermatol.* **18**, 237 (2017).
21. R.F. El-kased, R.I. Amer, D. Attia, and M.M. Elmazar: Honey-based hydrogel: In vitro and comparative in vivo evaluation for burn wound healing. *Sci. Rep.* **7**, 9692 (2017).
22. D.S. Choi, S. Kim, Y. Lim, H. Gwon, J.S. Park, Y. Nho, J. Kwon, and C. Honey: Hydrogel incorporated with chestnut honey accelerates wound healing and promotes early HO-1 protein expression in diabetic (*d*b/*d*b) mice. *Tissue Eng. Regener. Med.* **9**, 36 (2012).
23. J. Majtan: Honey: An immunomodulator in wound healing. *Wound Repair Regen.* **22**, 187 (2014).
24. T. Wang, X.K. Zhu, X.T. Xue, and D.Y. Wu: Hydrogel sheets of chitosan, honey and gelatin as burn wound dressings. *Carbohydr. Polym.* **88**, 75 (2012).
25. W.A. Sarhan and H.M.E. Azzazy: High concentration honey chitosan electrospun nanofibers: Biocompatibility and antibacterial effects. *Carbohydr. Polym.* **122**, 135 (2015).

https://doi.org/10.1557/jmr.2018.202 Published online by Cambridge University Press

26. J. Tavakoli and Y. Tang: Honey/PVA hybrid wound dressings with controlled release of antibiotics: Structural, physico-mechanical and in-vitro biomedical studies. *Mater. Sci. Eng., C* **77**, 318 (2017).
27. A. Chaudhury, S. Bag, A. Barui, P. Banerjee, and J. Chatterjee: Honey dilution impact on in vitro wound healing: Normoxic and hypoxic condition. *Wound Repair Regen.* **23**, 412 (2015).
28. L. Wang, M. Xu, L. Luo, Y. Zhou, and P. Si: Iterative feedback bio-printing-derived cell-laden hydrogel scaffolds with optimal geometrical fidelity and cellular controllability. *Sci. Rep.* **8**, 2802 (2018).
29. A. Ribeiro, M.M. Blokzijl, R. Levato, C.W. Visser, M. Castilho, W.E. Hennink, T. Vermonden, and J. Malda: Assessing bioink shape fidelity to aid material development in 3D bioprinting. *Biofabrication* **10**, 014102 (2017).
30. L. Ouyang, C.B. Highley, C.B. Rodell, W. Sun, and J.A. Burdick: 3D printing of shear-thinning hyaluronic acid hydrogels with secondary cross-linking. *ACS Biomater. Sci. Eng.* **2**, 1743 (2016).
31. L. Ouyang, R. Yao, Y. Zhao, and W. Sun: Effect of bioink properties on printability and cell viability for 3D bioplotting of embryonic stem cells. *Biofabrication* **8**, 035020 (2016).
32. S. Kyle, Z.M. Jessop, A. Al-sabah, and I.S. Whitaker: "Printability" of candidate biomaterials for extrusion based 3D printing: State-of-the-art. *Adv. Healthcare Mater.* **6**, 1700264 (2017).
33. M. Di Giuseppe, N. Law, B. Webb, R.A. Macrae, L.J. Liew, T.B. Sercombe, R.J. Dilley, and B.J. Doyle: Mechanical behaviour of alginate-gelatin hydrogels for 3D bioprinting. *J. Mech. Behav. Biomed. Mater.* **79**, 150 (2018).
34. K.R. Hixon, T. Lu, M.N. Carletta, S.H. McBride-Gagyi, B.E. Janowiak, and S.A. Sell: A preliminary in vitro evaluation of the bioactive potential of cryogel scaffolds incorporated with Manuka honey for the treatment of chronic bone infections. *J. Biomed. Mater. Res., Part B* **106**, 1918–1933 (2017).
35. R. Sarkar, A. Ghosh, A. Barui, and P. Datta: Repositing honey incorporated electrospun nanofiber membranes to provide anti-oxidant, anti-bacterial and anti-inflammatory microenvironment for wound regeneration. *J. Mater. Sci.: Mater. Med.* **29**, 31 (2018).
36. Y. He, F. Yang, H. Zhao, Q. Gao, B. Xia, and J. Fu: Research on the printability of hydrogels in 3D bioprinting. *Sci. Rep.* **6**, 1 (2016).
37. A. Schmitt, P. Rödel, C. Anamur, C. Seeliger, A.B. Imhoff, E. Herbst, S. Vogt, M. Van Griensven, G. Winter, and J. Engert: Calcium alginate gels as stem cell matrix-making paracrine stem cell activity available for enhanced healing after surgery. *PLoS One* **10**, 1 (2015).
38. B.E. Larsen, J. Bjørnstad, E.O. Pettersen, H.H. Tønnesen, and J.E. Melvik: Rheological characterization of an injectable alginate gel system. *BMC Biotechnol.* **15**, 1 (2015).
39. J.H.Y. Chung, S. Naficy, Z. Yue, R. Kapsa, A. Quigley, S.E. Moulton, and G.G. Wallace: Bio-ink properties and printability for extrusion printing living cells. *Biomater. Sci.* **1**, 763 (2013).
40. J. Park, S.J. Lee, S. Chung, J.H. Lee, W.D. Kim, J.Y. Lee, and S.A. Park: Cell-laden 3D bioprinting hydrogel matrix depending on different compositions for soft tissue engineering: Characterization and evaluation. *Mater. Sci. Eng., C* **71**, 678 (2017).
41. M. Di Giuseppe, N. Law, B. Webb, R.A. Macrae, T.B. Sercombe, R.J. Dilley, B.J. Doyle, and L.J. Liew: Journal of the mechanical behavior of biomedical materials mechanical behaviour of alginate-gelatin hydrogels for 3D bioprinting. *J. Mech. Behav. Biomed. Mater.* **79**, 150 (2018).
42. G. Kaklamani, D. Cheneler, L.M. Grover, M.J. Adams, and J. Bowen: Mechanical properties of alginate hydrogels manufactured using external gelation. *J. Mech. Behav. Biomed. Mater.* **36**, 135 (2014).
43. M. Ahearne, Y. Yang, and K. Liu: Mechanical characterisation of hydrogels for tissue engineering applications. *Tissue Eng.* **4**, 1 (2008).
44. K.R. Hixon, T. Lu, S.H. McBride-Gagyi, B.E. Janowiak, and S.A. Sell: A comparison of tissue engineering scaffolds incorporated with manuka honey of varying UMF. *BioMed Res. Int.* **2017**, 4843065 (2017).
45. B.A. Minden-Birkenmaier, R.M. Neuhalfen, B.E. Janowiak, and S. Sell: Preliminary investigation and characterization of electrospun polycaprolactone and manuka honey scaffolds for dermal repair. *J. Eng. Fibers Fabr.* **10**, 126 (2015).
46. M. Rajput, N. Bhandaru, A. Barui, A. Chaudhary, R.R. Paul, R. Mukherjee, and J. Chatterjee: Nano-patterned honey incorporated silk fibroin membranes for improving cellular compatibility. *RSC Adv.* **4**, 44674 (2014).
47. M. Funada, H. Hara, H. Sasagawa, Y. Kitagawa, and T. Kadowaki: A honey bee Dscam family member, AbsCAM, is a brain-specific cell adhesion molecule with the neurite outgrowth activity which influences neuronal wiring during development. *Eur. J. Neurosci.* **25**, 168 (2007).
48. A. Nordin, N.Q.A.V. Sainik, M.S. Zulfarina, I. Naina-Mohamed, A. Saim, and R. Bt Hj Idrus: Honey and epithelial to mesenchymal transition in wound healing: An evidence-based review. *Wound Med.* **18**, 8 (2017).
49. A. Oryan, E. Alemzadeh, and A. Moshiri: Biological properties and therapeutic activities of honey in wound healing: A narrative review and meta-analysis. *J. Tissue Viability* **25**, 98 (2016).
50. A.C. Daly, F.E. Freeman, T. Gonzalez-Fernandez, S.E. Critchley, J. Nulty, and D.J. Kelly: 3D bioprinting for cartilage and osteochondral tissue engineering. *Adv. Healthcare Mater.* **6**, 1700298 (2017).
51. K. Nair, M. Gandhi, S. Khalil, K.C. Yan, M. Marcolongo, K. Barbee, and W. Sun: Characterization of cell viability during bioprinting processes. *Biotechnol. J.* **4**, 1168 (2009).
52. P. He, J. Zhao, J. Zhang, B. Li, Z. Gou, M. Gou, and X. Li: Bioprinting of skin constructs for wound healing. *Burn. Trauma* **6**, 5 (2018).
53. A. Barui, P. Banerjee, A. Chaudhary, S. Conjeti, B. Mondal, S. Dey, and J. Chatterjee: Evaluation of angiogenesis in diabetic lower limb wound healing using a natural medicine: A quantitative approach. *Wound Med.* **6**, 26 (2014).

https://doi.org/10.1557/jmr.2018.202 Published online by Cambridge University Press